DYNAMICAL CHARACTERISTICS OF A PLANETARY PENETRATOR

H. Shiraishi[*], K. Suzuki[†], S. Tanaka[*],
M. Hayakawa[*], A. Fujimura[*], and H. Mizutani[*]

Abstract

We have developed an acceleration data acquisition system (an accelerometer and its electronics) during the course of development of the Japanese LUNAR–A penetrator mission, and we evaluated the performance and calibration properties on a series of impact tests with full size models. From the accelerometer record record, the impact velocity and the penetration path length of lunar penetrator are derived. Some prototype models carrying a data acquisition system were fired toward lunar analogue soil, and three–component acceleration data were obtained for a non–zero attack angle impact. The results indicate that the torque applied to the penetrator in case of an impact with a finite attack angle changes the penetration characteristics (penetration path length and inflection angle) significantly. The measured axial acceleration data indicate that the data acquisition system can provide the impact velocity and the penetration path length with sufficient accuracy, while the normal acceleration data suggest that the lunar penetrator will experience large shearing forces when it impacts with non–zero attack angle. We have also developed a numerical simulation code describing the penetration dynamics into the soil target, with emphasis on the influence of non–zero attack angle impact. Combining the results of penetration characteristics and measured acceleration data, we investigated the deceleration history and penetration trajectory predicted from model calculation.

1 Introduction

A hard landing probe (penetrator) has been thought to be a very useful tool to establish network stations on a planetary surface and sub–surface, because it provides light–weight and cost–effective capabilities of deploying scientific instruments. A long–lived network science by penetrators gives unique possibilities for monitoring global scale phenomena and for studies requiring simultaneous measurements (seismic, geodetic, magnetic, and

[*] *Institute of Space and Astronautical Science, Japan Aerospace Exploration Agency, Yoshino-dai 3-1-1, Sagamihara, Kanagawa 229-8510, Japan*
[†] *Graduate School of Frontier Sciences, University of Tokyo, Chiba 277-8562, Japan*

meteorological observations) from several sites in one mission. In addition, utilization of penetrators for planetary explorations has some advantages over soft landing probes. A penetrator will allow us to deliver scientific instruments into the planetary subsurface for *in situ* chemical analysis and/or heat–flow measurements; otherwise those measurements would require drilling holes from the surface. *In situ* geochemical measurements with higher resolution can also provide ground truth of remotely sensed data.

For the reasons cited above, several planetary missions using a penetrator system have been long proposed and developed. ISAS/JAXA (Institute of Space and Astronautical Sciences, Japan Aerospace Exploration Agency) of Japan plans to undertake a lunar mission named as LUNAR–A. The main objective of the LUNAR–A mission is to explore the lunar interior using seismometry and heat–flow measurements (Mizutani, 1995; Mizutani et al., 2003). The LUNAR–A penetrator mission is the first demonstration to implement a geophysical network and to investigate the internal structure of the Moon by an unmanned space probe.

To apply a penetrator system for planetary explorations, the most significant technical issue is an achievement of the shock-durability of the onboard instruments at the high–speed impact process. Thus, we need to know the impact load and penetrator movement during impact penetration for the structural make–up of a tough body and for a shock resistant hardware design, with an adequate strength and as light–weight as possible. Also, the maximum load conditions of flexure modes (compression, shear and bending) will supply helpful guidelines of the layout and potting procedure for manufacturing. Furthermore, the penetrator and onboard instruments must be deployed on the planetary surface at an adequate depth and a stop angle suitable for the later scientific observation and for its long–term remote operation. Anyway, the development of the penetrator for planetary exploration requires better understanding of the penetration dynamics into geological materials.

The LUNAR–A penetrator is equipped with a shock accelerometer as one of the science instruments, in order to measure the deceleration during penetration into the lunar surface. The record of the accelerometer gives the impact velocity and the penetration path length of the lunar penetrator by integrating over time. It is important for the data reduction of the seismic and the thermal experiment, as well as for the operational plan. We have developed an acceleration data acquisition system (an accelerometer and its electronics) for application on the LUNAR–A mission and evaluated the performance and calibration properties of the system during a series of impact tests. We have also developed a numerical simulation code describing the penetration dynamics into the soil target, including the effect of the initial attack angle (angle between body axis and velocity vector). In this paper, we report on experimental and numerical methods for the study of penetration dynamics and present some results from impact acceleration data and model calculations.

2 LUNAR–A penetrator and its deployment sequence

LUNAR–A penetrator is a missile–shaped instrument carrier and is planned to have 76 cm in length, 14 cm in maximum diameter, and about 14 kg in weight. It contains as

scientific instruments a two–component seismometer and a heat–flow probe, together with electronics, batteries, an accelerometer, a tiltmeter, and a radio–communication system. The tiltmeter is used to know the attitude of the penetrator that comes to rest in the lunar surface layer. The outer case is made from CFRP, and its inside is solidified by a mixture of epoxy resin and glass micro–balloon.

The mission scenario at the deployment phase on the moon is as follows (Yamakawa et al., 1994). The LUNAR–A spacecraft orbiting in a 45 km to 200 km elliptical orbit releases the LUNAR–A Penetrator Module (LPM), which consists of a penetrator, a de–orbit motor and an attitude control unit. Then, the LPM will transfer into a lower orbit due to the tangential velocity provided at the separation. Descending to a perilune altitude of 25 km, the orbital velocity of the LPM is cancelled by activating the de–orbit motor, which is followed by a free fall toward the lunar surface. During the free fall phase, the angular momentum vector of the LPM is reoriented by 90° to attain the normal incidence to the surface by the so–called rhumb line control (Morita et al., 1995). Finally, after the separation of the de–orbit motor and attitude control unit, the penetrator collides vertically with the lunar surface at a velocity of 300 m/s or less. As will be shown later, the LUNAR–A penetrator will experience a peak deceleration exceeding a few thousand G (in this paper, G refers to the average value of the acceleration of gravity on the surface of the Earth, 9.8 m/s^2), and penetrate to a depth of 2 to 3 m into the lunar surface layer, which consists of a mixture of granular soil and rock fragments estimated to be about 10 m thick.

Although the impact angle on the lunar surface is nominally designed to be 90° from the horizontal direction, there always exists a possibility that the lunar penetrator will hit on the Moon's surface at oblique incidence and with a finite attack angle. This will inevitably occur due to a possible misalignment of the separation mechanism w.r.t. the carrier spacecraft, slight errors of the motor ignition and the attitude control of LPM, and other influences. In particular, a large attack angle at impact is expected to result in a deflection of the penetration trajectory from the normal, and to provide a shock environment different from the case of normal incidence. This is because rotational torque will be applied to the penetrator by normal forces acting on the tip just after the initial contact. At this time, the LUNAR–A penetrator might be subject to severe normal acceleration due to shearing forces. Although great care to minimize the initial attack angle is taken in the design of the separation mechanism and the attitude control system, the normal incidence with zero attack angle can probably not be achieved. A maximum attack angle of 8° at impact must be accepted on the LUNAR–A mission. Therefore, we have developed a ground test facility to simulate such an impact condition and made penetration tests.

3 Experimental set–up

A series of impact tests for the final design of the LUNAR–A penetrator has been conducted using a gun with caliber 155 mm. The test facility is schematically shown in Figure 1. The gun barrel is a single stage rifle gun about 4 m in length and installed so that a projectile is shot horizontally. A prototype model penetrator is accelerated by the gun

barrel up to 300 m/s with a spin rate of about 10 Hz, and it impacts at normal incidence along the long–axis of a sand container, which is a 3.0 – 4.0 m sized steel box. During the free flight, the attitude of penetrator is slightly disturbed due to the aerodynamic instability, and the penetrator hits onto an opening of the sand container with a finite attack angle with respect to the flight direction. Both the impact velocity and the initial attack angle are measured stereoscopically using two high–speed video cameras.

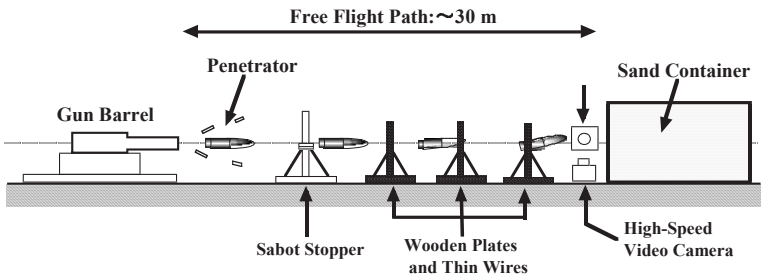

Figure 1: Schematic illustration of the entire test facility.

The surface on the Moon is covered by a debris blanket, the so–called *lunar regolith*, which completely hides the underlying bedrock. The lunar regolith consists of a mixture of fine dust, granular soil and rock fragments (Carrier et al., 1991). Because the mechanical properties of the target material could be essential parameters affecting the dynamic resistant force and the penetration characteristics, it is important to prepare a target having similar mechanical properties to those of the lunar regolith. Therefore, we prepared dry sand or analogue soil with the same size distribution as measured for returned lunar soil samples. A big sample of analog soil (70 tons in weight) was filled into the sand container, whose front end had a circular hole with diameter 40 cm covered by polyurethane foam of 60 cm in thickness, through which the penetrator impacted the soil sample. We controlled the degree of compaction so that the bulk density and hardness of the analogue soil were as close as possible to the values known from lunar regolith samples. The bulk density of the analogue soil in the sand container was estimated to be 1700 – 1900 kg/m^3. To secure the reproducibility of the experiments, the hardness of the analogue soil was monitored by a static hardness test using a cone penetrometer similar to that of the soil mechanics experiments on the Apollo missions. For more detailed information on the size distribution of the simulated lunar soil and the recorded hardness data, see Shiraishi et al.(2000). The size distribution of the lunar regolith at the Apollo landing sites has been described in Carrier et al.(1991) and the references given therein.

A projectile penetrator equivalent to the flight–model is of a cylindrical shape with a truncated ogive–nose and a maximum diameter of about 140 mm, and fabricated from A–7075 aluminum or from CFRP, as shown in Figure 2. Since the initiation of the development of the LUNAR–A penetrator, a large number of impact experiments have been conducted using scaled models having the base diameters of 15 mm, 30 mm, 50 mm, and 120 mm, respectively. The scaled models with several different nose shapes and

body designs were fired, and they impacted into simulated lunar surface material. As a result, the combination of a truncated ogive nose and a cylindrical part was adopted as the configuration of the outer case to satisfy both scientific and engineering requirements. Our previous studies had shown that the truncation of the nose tip was efficient to stabilize the penetration orientation in case of non–zero attack impact, as compared with a no–truncation nose shape (Shiraishi et al., 2000).

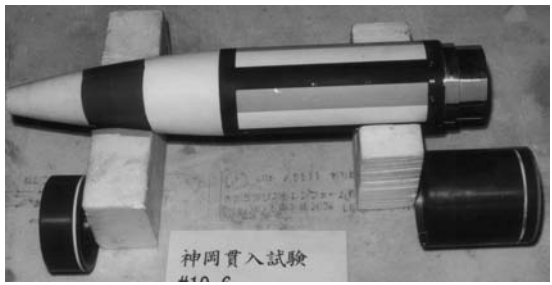

Figure 2: Photograph of a prototype penetrator (KGM–1 model) and a set of Al–alloy sabots.

The prototype models used in this study varied from 75 cm to 78 cm in length and 11.8 kg to 17.8 kg in weight, respectively, and they had a hollow space to mount instrument packages. Some test models carried the science instruments and other supporting equipment to verify their shock durability, and others were dummy test probes to establish the test conditions and to evaluate the penetration characteristics. Two Al–alloy sabots divided into three parts, 155 mm in diameter, were attached to the ogive–nose and rear end portion of the penetrator to hold properly the case structure in the barrel and to seal the propellant gas. Both the forward and afterward sabots were separated from the penetrator just after the launch and only the penetrator impacts into the sand container.

4 Acceleration data acquisition system

To date, to develop an acceleration data acquisition system onboard the LUNAR–A penetrator, we have made impact tests using scale models and investigated the shock durability of electrical components. Furthermore, the functionality of electric circuitry and the performance of various types of shock accelerometers were investigated. Based on these test results, the most suitable sensors and their electronics onboard the LUNAR–A penetrator have been already designed. In this study, to verify the hardware design and to evaluate the measurement accuracy under the actual flight conditions, we have specifically developed a data acquisition system. Although the data acquisition system onboard the prototype model is virtually equal to the flight model version, it can measure the normal acceleration perpendicular to the long axis of the penetrator body, as well as the axial acceleration. Thus we can investigate the effects of oblique incidence and the initial attack angle on the penetration dynamics. As mentioned earlier, the LUNAR–A penetrator is most likely to hit the lunar surface with oblique incidence and with a finite attack angle. This may affect both the penetration trajectory and the impact load significantly.

The system block diagram and the location of each component installed inside one of prototype models named as KCM–2 are shown in Figure 3 and Figure 4, respectively. Using the scale models, various types of sensors have been evaluated with respect to shock durability, zero shift, measurement accuracy, and so on. As a result, a piezoelectric sensor with an annular shear mode (Endevco Model 7255A–01 shock accelerometer) was selected for the LUNAR–A penetrator application. This sensor has a built–in mechanical filter system fabricated from a polymer, which is designed to effectively suppress high frequency inputs and to protect the sensing element from overstress.

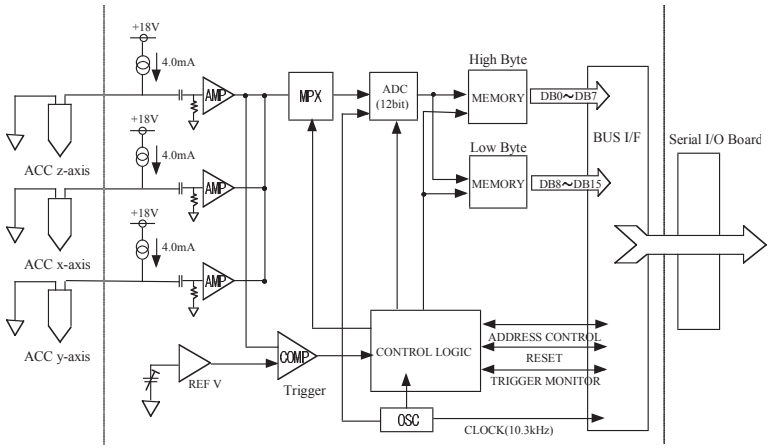

Figure 3: Schematic block diagram of the acceleration data acquisition system onboard the KCM–2 model.

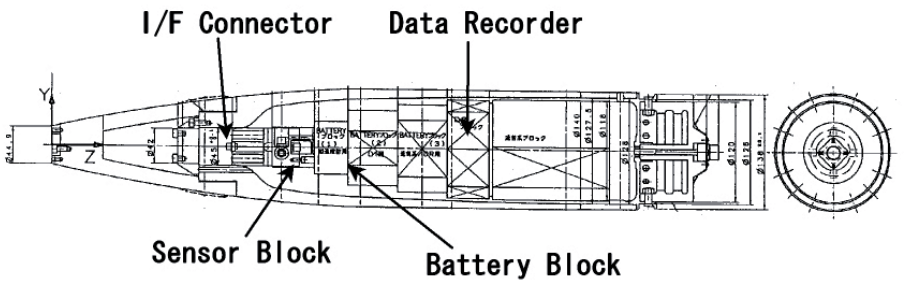

Figure 4: Internal configuration of a prototype model penetrator onboard the KCM–2 model.

The data recorder system onboard the prototype model is designed to upgrade the performance, with roughly 10 times higher resolution than the one built for the scale models. It has three separate input channels and can measure the two–component normal accelerations as well as the axial acceleration from the launch to the penetration into the sand.

Each accelerometer output is digitized by a multiplexer and a 12 bit A/D converter at a sampling rate of 10.3 kHz, and stored in a static memory. The buffer memory is 13000 words long at each channel, and it is frozen in about 800 msec after a preset voltage threshold is exceeded. Every channel has a dynamic range of -16000 to +16000 G to provide a resolution of about 8 G. The acquired data is read out by a personal computer through an interface board after recovering from the sand container. All the electrical components used have already been confirmed to withstand the shock acceleration of up to 10000 G on the impact experiments with the scale models. Just to be on the safe side, we also used an engineering model with lower–resolution, which passed through a large number of impact tests by scale models. A comparison of each data recorder system, including the flight–type model version onboard the LUNAR–A penetrator, is summarized in Table 1.

Table 1: Specifications of the data recorder system for acceleration measurements

Characteristics	Engineering model	Proto–type model	Flight–type model
A/D conversion	8 bits	12 bits	10 bits
Dynamic Range*	± 10000 G	± 16000 G	−10000 to +3300 G
Resolution*	80 G/DU	8 G/DU	13 G/DU
Sampling Rate	20.0 kHz	10.3 kHz	16.4 kHz

(*) Exact values are dependent on the sensitivities of individual accelerometers.

5 Penetration characteristics and recorded acceleration data

To accomplish the scientific observations by a penetrator system, it is crucial whether the penetrator could be deployed appropriately below the surface to satisfy both scientific and engineering needs. The LUNAR–A penetrator requires that it (the top of the penetrator) should rest in the lunar regolith at a depth deeper than 50 cm and at an attitude angle (angle between the penetrator body axis and the vertical) lower than 60°. The first requirement comes from the need of assuring temperature stability of the instruments and the second one comes from enabling measurement of the heat flow and allowing tele–communication between the penetrator and the orbiting mother spacecraft. Since the lunar regolith is relatively transparent to the radio–wave (Carrier et al., 1991), there will be essentially no attenuation of the radio signal from the antenna if the penetrator is buried at the depth of 1 to 5 m.

Figure 5 shows a cross sectional view of a penetrator that came to rest in the sand box, where the final location and the stop angle are projected onto the vertical plane. For this test run, the KBM–2 model (78.8 cm in length, 145 mm in diameter and 13.2 kg in weight) was used. It impacted at the velocity of 322 m/s and an attack angle of 5°. The projectile parameters and impact conditions are most similar to the actual flight ones among a series of test runs. In this test KBM–2 model penetrated 2.18 m from the impact point and came to rest with a 35° stop angle. In case of normal incidence with zero attack angle, it

is anticipated that the body axis of the penetrator at the rest position coincides closely with the impact direction. However, Figure 5 indicates that the existence of a finite attack angle at impact can easily result in the deflection of the penetration trajectory and in a highly inclined stop angle w.r.t. the vertical direction.

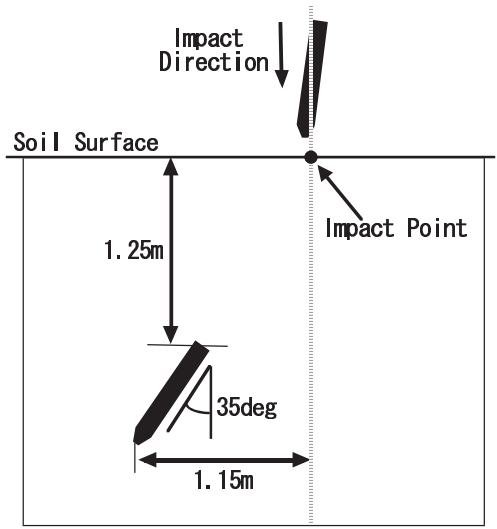

Figure 5: Schematic cross sectional view of the location and stop angle before and after impact penetration. The size of KBM–2 model penetrator is shown to scale.

Figure 6 is a photograph of a prototype model recovered after the impact penetration. For this test run, the KGM–1 model with a weight of 15.7 kg impacted with a velocity of 305 m/s and an attack angle of 8°. The streak pattern left on the body surface shows a distinctive feature. Two heavily scoured regions can be seen, not symmetric around the body axis. One is on the windward side of the ogive nose with respect to the pitch motion, and the other is on the windward side of the cylindrical part. The latter is scoured deeper toward the rear end. By contrast, no significant erosion can be seen on the leeward side of the cylindrical part. Considering the large stop angle and the asymmetric streak pattern around the body axis, the penetrator seems to have suffered a high normal acceleration or shearing force.

The variation of the stop angle with the initial attack angle is shown in Figure 7a. It indicates that an increase in attack angle at impact enhances the deflection of penetration trajectory from the impact direction. However, even if the lunar penetrator impacts at the worst case of 8° initial attack angle, the stop angle is anticipated to be within 60° from the normal direction.

Figure 7b shows the penetration path length with respect to the initial attack angle. As for

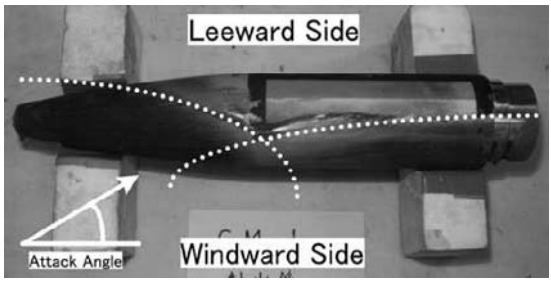

Figure 6: Photograph of the KGM–1 model penetrator after the impact penetration.

the vertical axis in Figure 7b, the mass–normalized penetration path length is introduced to eliminate the effect of different penetrator masses used in a series of impact tests. The mass–normalized penetration path length d_N is given by the following equation:

$$d_N = d_t \left(\frac{M_0}{m_t} \right) \tag{1}$$

where m_t is the mass of the prototype model used in a particular test run. d_t is the penetration path, which is defined as a straight line drawn from the impact point to the nose tip of the penetrator after it has come to rest in the sand container. M_0 is the mass of the LUNAR–A penetrator and is assumed to be 13.7 kg in this study. As the initial attack angle increases, the penetration path length decreases. However, even if the lunar penetrator impacts at the worst case of initial attack angle, it is anticipated that the rear end of the lunar penetrator will be deployed at a depth of 100 – 150 cm, ensuring an environment appropriate for the scientific observations as well as for data transmission.

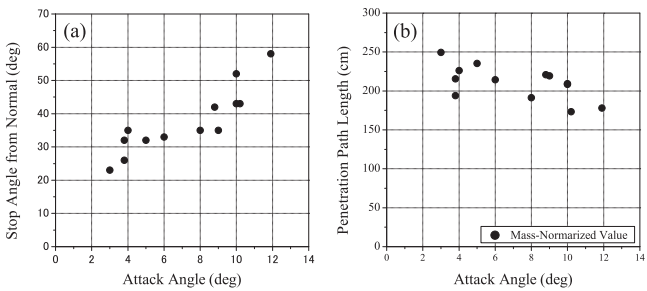

Figure 7: (a) Variation of the stop angle as a function of the initial attack angle. (b) Variation of the penetration path length with attack angle at impact. Only the results for cases where the projectiles impacted at velocities of 280 to 330 m/s are shown.

Figure 8 shows an example of three–axis acceleration profiles obtained during a series of tests. For this test run, the KGMDP–1 model with a weight of 12.7 kg was fired with a velocity of 306 m/s and impacted with the attack angle of 11°. The data recorder can make a measurement of the penetrator's structural response. At the shot timing from the gun barrel and just after the impact, high frequency responses shown in the axial and in the normal acceleration profiles are associated with separate vibrations of the penetrator case, which correspond to the compression mode (2.6 to 2.8 kHz) and to the bending mode (1.2 to 1.3 kHz), respectively. Figure 9a is another example of acceleration profiles. The KCM–2 model is 16.3 kg in weight, and it impacted with a velocity of 332 m/s and an attack angle of 6°. It penetrated 2.66 m and came to rest with a 34° stop angle. Just after the impact, the axial acceleration reaches its maximum value of 5000 G, while the normal acceleration, at which the accelerometer is mounted, records a maximum of 3000 G to 4000 G. Even with the initial attack angle of only 6°, the measured normal acceleration is very large and comparable to the axial one.

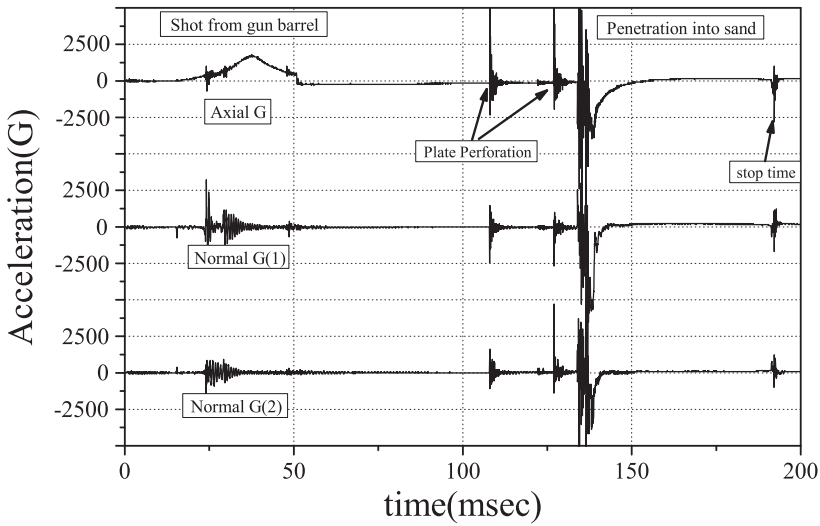

Figure 8: Three–axis acceleration profiles obtained for the KGMDP–1 model from shot to impact penetration.

This acceleration profile shows another notable feature. After the normal acceleration reaches its maximum value at about 4 msec from the impact, it suddenly decreases and vanishes almost at the only 8 msec. In the KCM–2 test run, the stop time is estimated to be about 40 msec from the axial acceleration and from the velocity variation as shown in Figure 9b. This indicates that the KCM–2 model was subject to shearing forces only at the early stage of penetration. The velocity by integrating the axial acceleration with time is 340 ± 2 m/s, while the impact velocity measured by the high–speed video cameras is 332 m/s. Since the maximum instrumental errors for the velocity measurement are estimated to be about 5%, they are in fairly good agreement with each other.

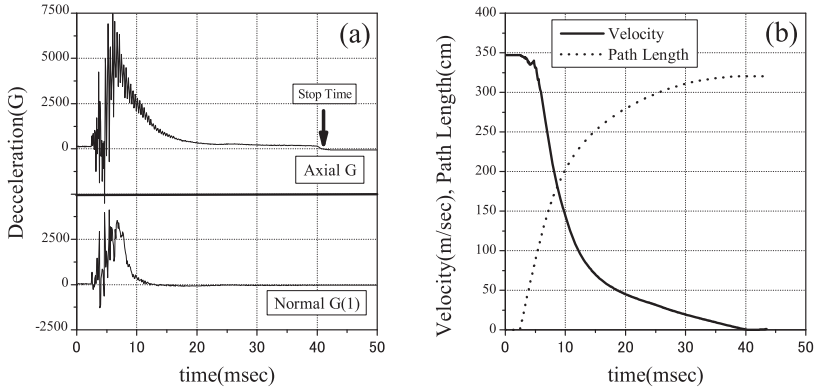

Figure 9: (a) Axial and normal acceleration profiles for the KCM–2 model and (b) variation of velocity and penetration path length obtained by integration of the acceleration signal over time.

6 Numerical simulation code

A numerical model describing the dynamics of the LUNAR–A penetrator into the lunar soil material and the load distribution applied to the body, including the effects of oblique impact and the initial attack angle, is presented. This numerical code has been developed to investigate the maximum load condition and to design the outer case of flight model with an adequate strength and at a minimum of weight. In the following, we describe the formulation of this numerical model.

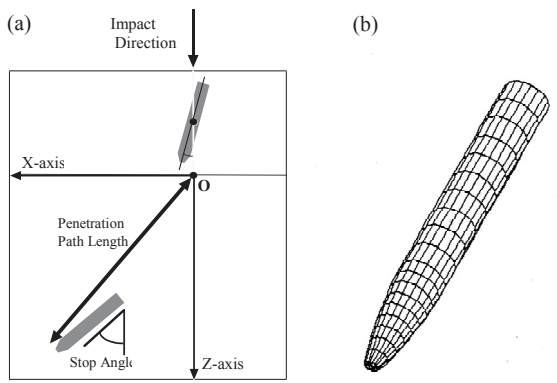

Figure 10: Schematic illustrations of (a) the coordinates for numerical simulation and (b) the panel method for calculating the force acting on the penetrator body.

1. The coordinates for this simulation are illustrated in Figure 10a. In this model, out–of–plane motion of the penetrator is neglected, that is, the three degrees of freedom equations of motion are given by,

$$m\frac{d^2x}{dt^2} = F_x, m\frac{d^2z}{dt^2} = F_z, I_{yy}\frac{d\omega}{dt} = M_y \tag{2}$$

where m, I_{yy} and ω are the penetrator mass, the moment of inertia and the angular velocity around y–axis, respectively. F_x and F_z represent the forces acting on the center of mass parallel to the x–axis and z–axis, respectively. M_y is the pitching moment around y–axis. They are solved numerically by using a 4^{th} order Runge–Kutta method with the initial impact conditions (i.e., impact velocity, impact angle and initial attack angle). The distribution of forces acting on the body surface from the soil is determined under the following assumptions, based on the modified Newtonian theory (Anderson, 1989).

2. At each time step, F_x, F_z, and M_y are computed by the panel method; the entire surface of the penetrator, including the base area, is divided into 57 longitudinal × 36 circumferential panels as shown in Figure 10b, and forces acting on each panel are calculated independently and summed vectorially to obtain F_x, F_z, and M_y.

3. The soil is in contact only with the panels in the windward side with respect to the direction of penetration. The forces only act on the panels where the following relation is satisfied,

$$\overrightarrow{V_L} \cdot \overrightarrow{n} < 0 \tag{3}$$

where $\overrightarrow{V_L}$ is the velocity vector of local soil flow on a panel and $\overrightarrow{n}$ is the outward normal vector of the panel.

4. The force acting on the panel to satisfy Equation (3) is decomposed into the normal component f_n and the tangential component f_t.

5. The normal force f_n is given by the equation,

$$f_n = \eta\rho {V_n}^2 + S_t \tag{4}$$

where ρ, V_n, and S_t are the bulk density of the soil, normal component of the local soil velocity to the panel, and the hardness of the uncompressed soil, respectively. This relation means that the dynamic pressure from the soil determines the normal force when it exceeds the hardness of soil at the high velocity regime. The static soil hardness S_t is important at the low velocity regime and is assumed to be constant, i.e. not dependent on the penetration velocity. The bulk density of the soil is also assumed to be homogeneous along the penetration trajectory and is taken as 1800 kg/m^3 in this study. The non–dimensional factor η is introduced to consider the hardening effect of the soil due to the dynamic pressure and is defined as a function of the transient velocity of the center of mass, $|\overrightarrow{V_{CG}}|$.

6. The tangential component f_t is assumed to be the frictional force between the panel and the soil, and it is given by using a sliding friction coefficient μ,

$$f_t = \mu f_n. \tag{5}$$

The direction of the tangential force of a panel coincides with the projection of the local soil velocity vector $\overrightarrow{V_L}$ onto the panel. The frictional force f_t becomes important when the translational velocity of the penetrator decreases to less than ∼30 m/sec.

7. The velocity vector of the local soil flow $\overrightarrow{V_L}$ at a panel is determined by superimposing the velocity vector of the center of mass $\overrightarrow{V_{CG}}$ and the rotational velocity,

$$\overrightarrow{V_L} = \overrightarrow{V_{CG}} + \epsilon \cdot (\overrightarrow{X} - \overrightarrow{X_{CG}}) \times (0, \omega, 0)^T \tag{6}$$

where $\overrightarrow{X}$ and $\overrightarrow{X_{CG}}$ represent the position of each panel and of the center of mass, respectively. The non–dimensional factor ϵ is a weighting factor of the rotational velocity to the translational velocity of the penetrator. It should be noted that the above model coincides with the straight Newtonian impact theory if both η and ω are set to 1.0.

8. In the above procedures, four unknown parameters η, ϵ, S_t, and μ are included. They are determined by fitting to the experimental data. The dynamic pressure factor η is determined by comparison with the axial acceleration data,

$$\eta = 1 + \frac{\alpha}{|\overrightarrow{V_{CG}}|} \tag{7}$$

where α is defined as a constant. Because ϵ determines the magnitude of damping to the pitch motion in case of a non–zero attack angle impact, a larger value of ϵ results in a smaller difference between the impact direction and the final stop angle. Thus, ϵ is determined as 0.9 so that it would satisfy the variation in the stop angle with the initial attack angle as shown in Figure 7a. As for the hardness of the uncompressed soil S_t, we take 2 MPa as an average from the resistant force data with cone penetrometer for the analogue soil. Finally, the coefficient of friction μ is determined to be 0.02 by fitting to the results on the variation in the penetration path length with impact velocity shown in Figure 7b. Based on the above assumptions, the distribution of forces from the soil is computed over the whole body surface at each time step.

7 Penetration dynamics

The axial and normal decelerations with time for the KCM–2 model impact predicted from the numerical simulation are indicated in Figure 11. This model calculation for both the axial and normal decelerations is in good agreement with the measured acceleration data.

This numerical code can predict the normal acceleration at an arbitrary location of the penetrator body and the time variation of the attack angle. Figure 12a shows the normal acceleration profiles at the locations of the ogive–nose tip, the center of mass, and the rear end, respectively. It indicates that the KCM–2 model experiences the same large normal acceleration as the axial one from the windward side and that the shearing forces become very severe at the ogive nose tip and at the rear end portion. This result is consistent with the fact that two heavily scoured regions were observed on the windward side of the ogive nose and of the rear end portion (see Figure 6b). As can be seen in Figure 12b, the initial attack angle is cancelled completely after only 10 msec from the impact, though it once increases suddenly just after the impact. An abrupt change of attack angle is most likely to be associated with the bimodal signature of normal acceleration, as pointed by the arrows in Figure 11b and Figure 12a.

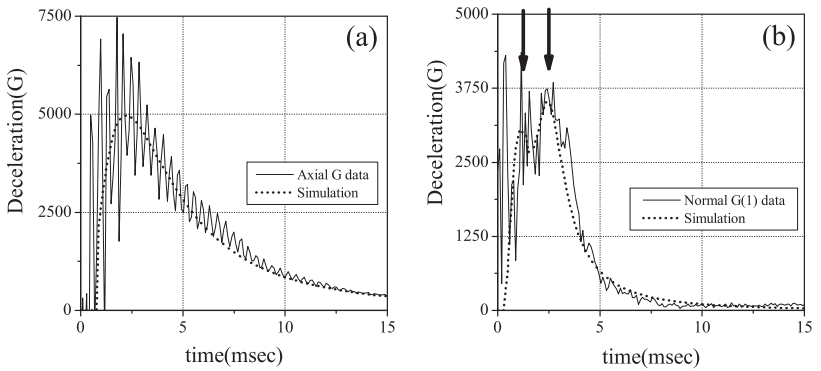

Figure 11: Deceleration time history predicted from the KCM–2 model calculation; (a) axial acceleration and (b) normal acceleration. The parameter α was set to 400.

Figure 13 shows the penetration trajectory of the KCM–2 model at every 1 msec time step predicted from the model calculation. This indicates that the trajectory of the KCM–2 model begins to bend in the neighborhood of the impact point and that it penetrates with increasing angle between body axis and velocity vector. However, it also indicates that an inflection of the velocity vector occurs while most of the KCM–2 body is still outside the soil target. And then, it seems that the increased attack angle is cancelled due to the fact that the KCM–2 model suffers a large normal acceleration on the rear end portion and that the deflection of penetration trajectory stops. Finally, the KCM–2 model penetrates during the main part of the trajectory with almost zero attack angle. This suggests that the real curved penetration path may not be very different from a straight path.

The double integration of axial acceleration over time gives the final penetration path length of 2.69 ± 0.05 m, while the measured path length of KCM–2 model is 2.66 ± 0.08 m. This means that even if the LUNAR–A penetrator would hit the lunar surface with non–zero attack angle, its penetration trajectory could be approximated as the straight path line. As mentioned earlier, the stop angle will be measured by the onboard tiltmeter. Therefore, by combining the data of accelerometer and tiltmeter, we will be able to

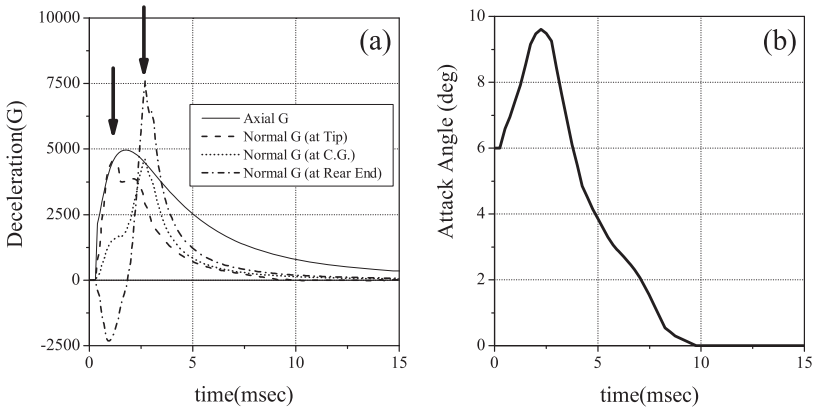

Figure 12: (a) Deceleration profiles calculated at the various stations of KCM–2 model and (b) the time variation of the attack angle.

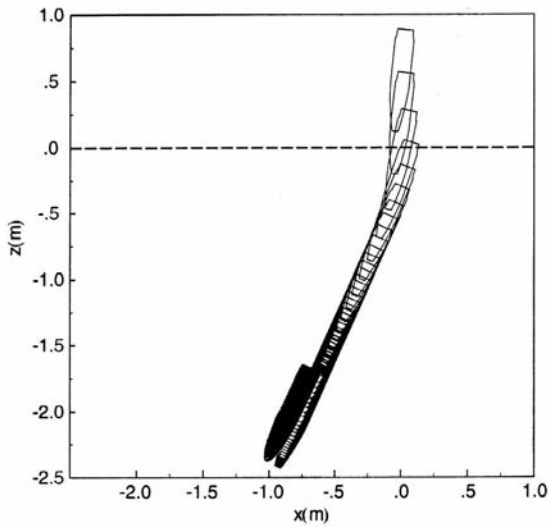

Figure 13: Penetration trajectory of KCM–2 model at every 1 msec time step predicted from the model calculation. For comparison, the final location and stop angle observed in the actual KCM–2 model test are also shown in a shaded area. The broken line depicts the surface of soil target.

estimate the depth of emplacement and the location with respect to the crater produced at the impact point. The range of possible locations might be determined with an accuracy of 10 to 20 cm, though it is dependent on the impact angle of the lunar penetrator and possibly unexpected local topography at the impact site. An accurate estimation

of the depth of emplacement and of the location relative to the impact point could be important to interpret the data gathered by science instruments and to know immediately the possible number of transmissions and the geometry of passes, in which the telemetry system onboard the LUNAR–A penetrator can transmit the data to the carrier spacecraft.

Acknowledgments

Part of the acceleration data acquisition system used in this study was manufactured by the former Nissan Motor Corporation. The technical staffs at the Nissan Motor are greatly acknowledged for their dedicated work during the manufacture of the instruments and their ground tests. We are also very grateful to the members of ISAS engineering groups for their unselfish contribution of the engineering aspect of the LUNAR–A mission.

References

Anderson J.D.: Local surface inclination methods. iIn *Hypersonic and High Temperature Gas Dynamics*, edited by the author, New York, McGraw–Hill, 45–75 (1989).

Carrier III W.D., Olhoel G.R., Mendell W.: Physical properties of the lunar surface. In: *Lunar Sourcebook: A User's Guide to the Moon*, edited by G.H. Heiken, D.T. Vaniman, and B.M. French, Cambridge, Cambridge Univ. Press, 475–594 (1991).

Mizutani H.: Lunar interior exploration by Japanese lunar penetrator mission, LUNAR–A. *J. Phys. Earth* **43**, 657–670 (1995).

Mizutani H., Fujimura A., Tanaka S., Shiraishi H., Nakajima T.: LUNAR–A mission: goals and status. *Adv. Space Res.* **31**, 2315–2321 (2003).

Morita Y. et al.: Attitude control systems of the LUNAR–A penetrator. In: A Collection of Technical Papers, *ISAS 5'th Workshop on Astrodynamics and Flight Mechanics*, Institute of Space and Astronautical Sciences, Sagamihara, Japan, 71–76 (1995).

Shiraishi H., Tanaka S., Hayakawa M., Fujimura A., Mizutani H.: Dynamical characteristics of planetary penetrator: effect of incidence angle and attack angle at impact. *Institute of Space and Astronautical Sciences Report* No. 677, p. 21 (2000).

Yamakawa H. et al.: LUNAR–A trajectory description. *19'th International Symposium on Space Technology and Science*, Yokohama, Japan, ISTS 94–c–30 (1994).